

Project of X-ray optical scheme of a lithograph with a transmissive dynamic mask and a synchrotron radiation source

© I.V. Malyshev,¹ N.I. Chkhalo,¹ S.N. Yakunin^{2,3}

¹ Institute of Physics of Microstructures, Russian Academy of Sciences, 607680 Nizhny Novgorod, Russia

² Scientific Research Center Kurchatov Institute, 123182 Moscow, Russia

³ NRC Kurchatov Institute and Institute of Crystallography RAS 119333 Moscow, Russia
e-mail: ilya-malyshev@ipm.sci-nnov.ru

Received May 3, 2023

Revised May 3, 2023

Accepted May 3, 2023

The paper proposes an X-ray optical scheme of a lithograph with a transmissive dynamic mask and a synchrotron radiation source. The image of a dynamic mask in the form of holes of small diameter is transferred with a decrease to a plate with a resist using a Schwarzschild projection lens. The formation of a topological pattern will occur due to the coordinated operation of the system for scanning a plate with a resist and a microelectromechanical system of a transmissive type. Objectives with a reduction of 10 and 20 times for obtaining 10–20 nm images of 200 nm holes of the dynamic mask are considered. The scheme of illumination of the mask is calculated, which provides uniform illumination on a field of $10 \times 10 \text{ mm}^2$. For the synchrotron Siberia-2 of the KISI on a bending magnet, the expected productivity of the lithograph will be up to 1/14 of a plate with a diameter of 100 mm per hour.

Keywords: X-ray lithography, X-ray optics, multilayer mirror, synchrotron radiation, aberrations.

DOI: 10.61011/TP.2023.07.56638.111-23

Introduction

The use of synchrotron radiation sources for X-ray or extreme ultraviolet (EUV) lithography, in particular at wavelengths 11.3 and 13.5 nm, has been considered for a long time [1–5]. The first experimental lithographic drawings were obtained using synchrotrons [1,2]. However, they have not yet been broadly applied for a number of reasons, including due to insufficient radiation power in the spectral bandwidth of the X-ray optical system [3]. Recently, a new type of synchrotron source with high power was proposed for EUV lithography tasks in the paper [6]. A synchrotron with a storage ring diameter of 160 m is proposed to obtain coherent EUV radiation of the kilowatt level. The electron beam in it is modulated by a laser with a wavelength of 257 nm using the microgrouping method, which theoretically makes it possible to obtain coherent radiation at a wavelength of 13.5 nm with an average power of 2.5 kW.

The productivity of the lithographic process is sidelined in the case of maskless EUV lithography [7,8], and experiments can be carried out on existing synchrotrons. In this paper we consider the X-ray optical circuit of the EUV lithograph using a synchrotron source and a dynamic mask for transmission [9]. The calculation is made for KSRS synchrotron [10]. The productivity of the lithograph can be improved by installing it on Russian synchrotrons under construction with undulator sources SKIF [11,12] and SILA [13].

1. Calculation of the optical circuit

The optical circuit of the lithograph was calculated using Zemax program. The beam coming out of the synchrotron, propagating in the horizontal plane, is reflected downwards by the two-mirror system and illuminates a dynamic mask (hereinafter „mask“), working for transmission and placed in the plane of the lens objects (Fig 1). Mask image 3 is constructed with a two-mirror lens 4 with a reduction of $\times 10$ or $\times 20$ on a plate with a resist 7. The topological pattern on the resist is obtained through the coordinated movement of the plate with the resist on the scanner table and the controlled opening–closing of the mask holes.

The lithograph has the following workflow: the opening of some holes of the mask, the illumination of the resist simultaneously with its movement to print tracks. Next, all the holes of the mask are closed to draw a different topology in a different place of the resist, the resist is shifted, then a new set of holes is opened, and the illumination with the offset of the resist continues. It will be possible to form any topological pattern in this way. Opening–closing of the mask holes will be performed by the supply of voltage to the shutters of the holes of the dynamic mask [9].

The description of the circuit will begin along the course of the rays, i.e. from the source to the resist. We took the parameters of the synchrotron source from the „Large Storage“ of Kurchatov Synchrotron as a basis [10]. Source size: $\sigma_x = 700 \mu\text{m}$, $\sigma_y = 45 \mu\text{m}$. The beam cross section at a distance of 11 m from the source for the working

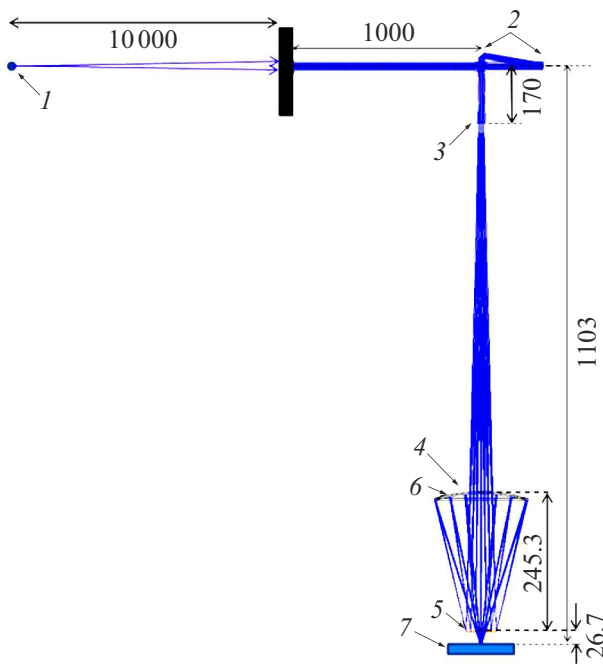


Figure 1. Optical scheme of an 11.2nm EUV lithograph on a synchrotron: 1 — synchrotron source, 2 — two-mirror mask illumination system, 3 — dynamic mask $10 \times 10 \text{ mm}^2$ for clearance with 200-nm holes, 4 — 10x lens, NA= 0.3, 5 — mirror M1, 6 — mirror M2, 7 — plate with a resist on the scanner. Notations in millimeters.

wavelength of 11.2nm is shown in Fig. 2, *a*. It has an intensity distribution in the area of $44 \times 22 \text{ mm}$, so the minimum size of the first mirror tilted at 45° is equal to $44 \times 32 \text{ mm}$.

The problem of a two-mirror illumination system (Fig. 3) — create a quasi-uniform intensity distribution on the dynamic mask with the size $10 \times 10 \text{ mm}^2$ (Fig. 2, *b*) with minimal divergence, i.e. to form the maximum possible plane-parallel beam. Then, the radiation will come out of the holes slightly divergent due to diffraction on the holes of the mask and get into the inlet aperture of the lens.

Toroid mirror 1 in Fig. 3 compresses the beam horizontally (along *X*) and stretches vertically so that the entire area $10 \times 10 \text{ mm}^2$ on the mask is illuminated with the most uniform intensity field. The convex mirror 2, working in tandem with the toroid, makes the beam close to plane-parallel. As a result, the residual geometric divergence along the *Y* axis and convergence along the *X* axis (Fig. 3) have numerical apertures $\text{NA} = 0.013 - 0.015$, i.e. approximately 5 times less than the diffraction divergence of radiation transmitted through 200-nanometer holes of the dynamic masks, therefore, have almost no effect on the angular intensity distribution in the diffracted beam. The proposed EUV lithograph circuit can be implemented on any synchrotron by slightly changing the parameters of the two-mirror illumination system in order to create a quasi-collimated beam with an uniform field on a dynamic mask from any synchrotron beam.

The radiation passes through the holes in the mask, diffracts on them and enters the projection lens, which builds a reduced image of the mask on the resist. When diffraction occurs on round holes of a thin mask, 84% of the radiation is contained in the central diffraction peak (Fig. 4). Its numerical aperture NA is calculated using the following formula:

$$\text{NA} = 1.22 \cdot \lambda / D_{\text{hole}}, \quad (1)$$

and in our case for $\lambda = 11.2 \text{ nm}$ and $D_{\text{hole}} = 200 \text{ nm}$ is 0.068. A divergent beam with an intensity distribution of the numerical aperture shown in Fig. 4 will come out from each hole of the dynamic mask due to diffraction.

Fig. 4 shows that the numerical aperture of $\text{NA} = 0.03$ and 0.02 beams coming out of the holes of the mask contains 48 and 25% of radiation, respectively. The lenses considered in this paper, located along the path of the rays after the dynamic mask (Fig. 1), have an input numerical aperture of $\text{NA}_{\text{in}} = 0.03$ (for a lens $\times 10$ with $\text{NA}_{\text{out}} = 0.3$) and $\text{NA}_{\text{in}} = 0.02$ (for a lens $\times 20$ with $\text{NA}_{\text{out}} = 0.4$), so they will capture 48 and 25% of the radiation, respectively. We will need these values when evaluating the productivity of the lithograph.

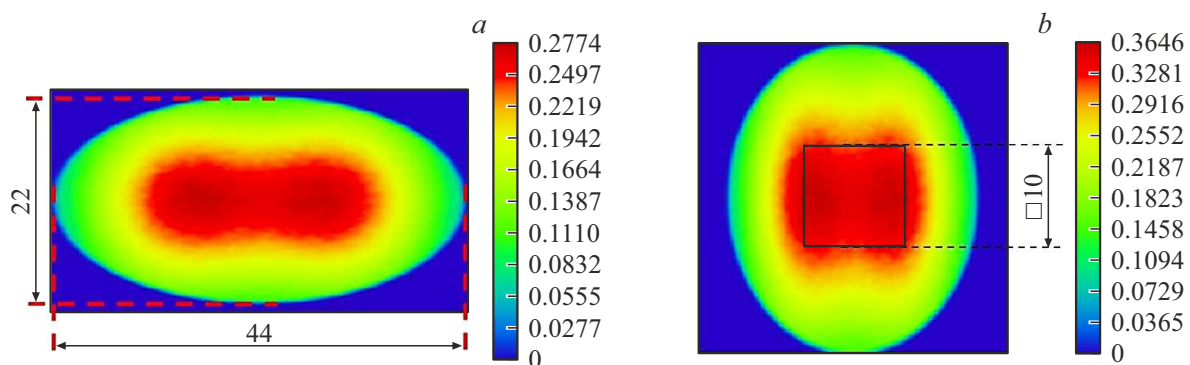


Figure 2. *a* — beam cross section at a distance of 11 m from the source for an operating wavelength of 11.2nm; *b* — a spot of illumination of the dynamic mask by a synchrotron beam formed by a two-mirror illumination system. Notations in millimeters.

Let's proceed to the calculation of the projection lens. The lens should have a reduction of $\times 10$ and $\times 20$, respectively, to obtain 20- and 10-nm resolutions. Figure 5 shows the X-ray optical circuit of the lens and the main dimensions. The thickness of the mirrors, the possibility of placing between the M1 mirror and the plate with the „autofocus“ resist to control the position of the plate relative to the projection lens was taken into account for the development of the lens. The length of the lens from the aperture to the resist is 933 mm, so the vacuum chamber of the lithograph turns out to be relatively compact.

The field of view of the projection lens is quite large, $10 \times 10 \text{ mm}^2$, therefore, to ensure diffraction image quality over the entire field, both mirrors have an aspherical shape of the reflecting surface. The aspherization profiles of mirrors M1 and M2 are described by the formula

$$z = \frac{cr^2}{1 + \sqrt{1 - (1+k)c^2r^2}} + \alpha_2 r^2 + \alpha_4 r^4 + \alpha_6 r^6 + \alpha_8 r^8 + \alpha_{10} r^{10} + \alpha_{12} r^{12}, \quad (2)$$

where the surface of the mirror M1 is set by the parameters:

$$\begin{aligned} k &= -0.36032, & c &= 1/R_{\text{vertex sphere}} = 1/56 \text{ (mm}^{-1}\text{)}, \\ \alpha_2 &= -0.000716, & \alpha_4 &= -4.125 \cdot 10^{-7}, \\ \alpha_6 &= -4.485 \cdot 10^{-11}, & \alpha_8 &= -5.393 \cdot 10^{-15}, \\ \alpha_{10} &= -1.175 \cdot 10^{-18}, & \alpha_{12} &= -4.997 \cdot 10^{-23}, \end{aligned}$$

r ranges from 0 to 22.5 mm; the surface of the M2 mirror is set by the following parameters:

$$\begin{aligned} k &= -0.01276, & c &= 1/R_{\text{vertex sphere}} = 1/294.4 \text{ (mm}^{-1}\text{)}, \\ \alpha_2 &= -1.0 \cdot 10^{-4}, & \alpha_4 &= -2.762 \cdot 10^{-10}, \\ \alpha_6 &= -1.303 \cdot 10^{-15}, & \alpha_8 &= 7.161 \cdot 10^{-20}, \\ \alpha_{10} &= -7.599 \cdot 10^{-24}, & \alpha_{12} &= -3.077 \cdot 10^{-28}, \end{aligned}$$

r ranges from 0 to 83.5 mm.

The lens provides diffraction-limited image quality over the entire field of view (Fig. 6, 7). For incoherent radiation, the diameter of the hole images was 16 nm at the 0.7 level and 22 nm at the 0.5 level.

The images of the holes are narrowed to 19 nm at the 0.5 level and 14 nm at the 0.7 level (Fig. 8) for coherent light, which can be obtained using synchrotrons with undulatory sources, i.e. interference of spherical waves diverging from the holes occurs, which in this case leads to a narrowing of the peaks intensity in the image.

Lens distortion $\times 10$ at the edge of the 10-mm field the field of view was 7 nm in the image plane (Fig. 9), which can be compensated by the movement of the table with a resist along the arc during scanning.

Figures 10 and 11 show images with a lens $\times 20$, NA=0.4. Fig. 11 shows that the size of the images of

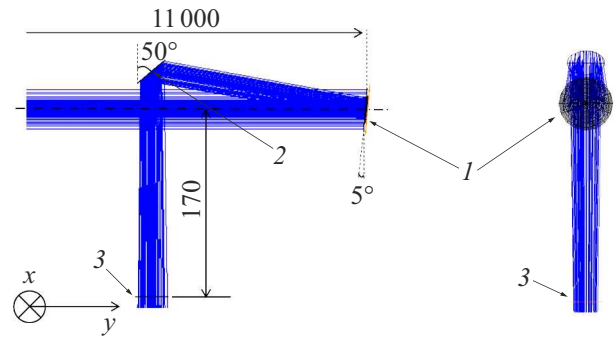


Figure 3. Two-mirror illumination system: *a* — side view, *b* — front view. *1* — toroid mirror ($R_{\text{horiz}} = -1500 \text{ mm}$ (concave), $R_{\text{vert}} = 5000 \text{ mm}$ (convex), $D = 46 \text{ mm}$), *2* — convex mirror ($R_{\text{horiz}} = 2600 \text{ mm}$, $D = 32 \text{ mm}$), *3* — dynamic mask. Notations in millimeters.

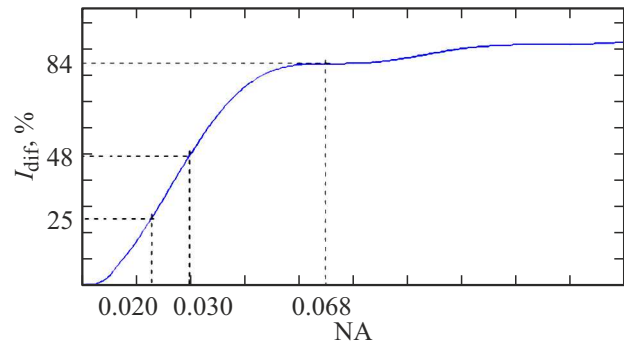


Figure 4. Distribution of the intensity of the radiation diffracted at the 200-nm hole from the numerical aperture (Fraunhofer zone).

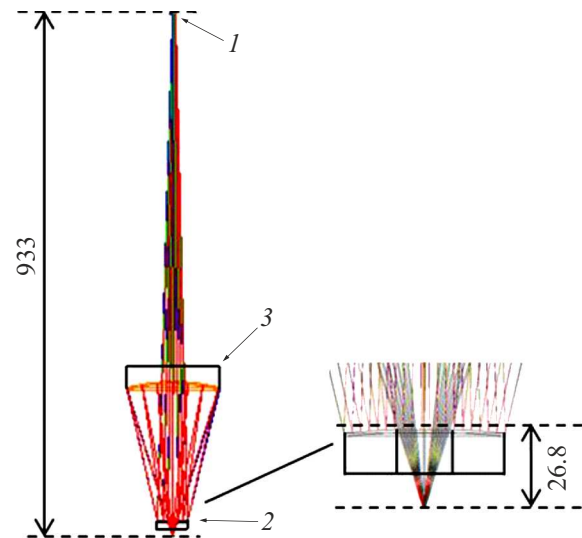


Figure 5. Lens $\times 10$, NA=0.3. *1* — dynamic mask, *2* — mirror M1 ($D_{\text{optical}} = 55 \text{ mm}$, $R_{\text{nearest sphere}} = 279 \text{ mm}$, $PV_{\text{aspheric}} = 5.36 \mu\text{m}$), *3* — mirror M2 ($D_{\text{optical}} = 167 \text{ mm}$, $R_{\text{nearest sphere}} = 312.2 \text{ mm}$, $PV_{\text{aspheric}} = 6.37 \mu\text{m}$).

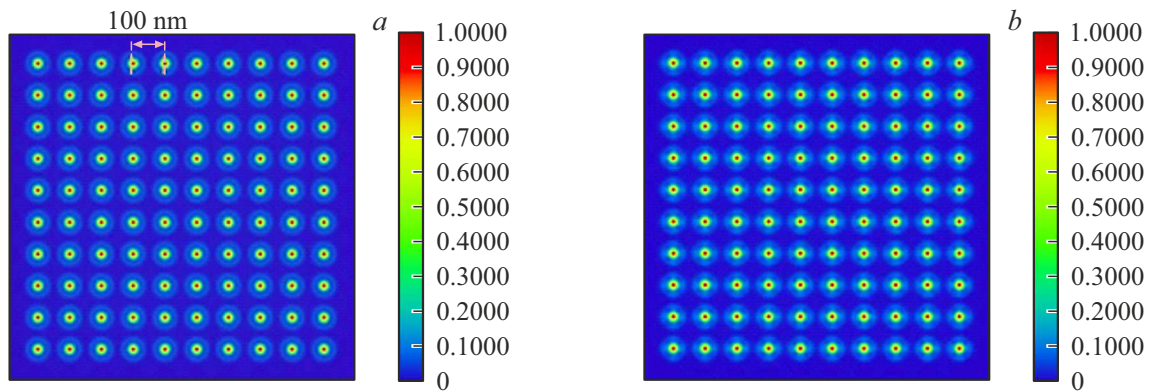


Figure 6. The image of 200-nm holes of a dynamic mask on a resist in the center (*a*) and at the edge (*b*) of the field of view $10 \times 10 \text{ mm}^2$. Lens $\times 10$, $\text{NA} = 0.3$, $\lambda = 11.2 \text{ nm}$. The synchrotron radiation was set incoherent.

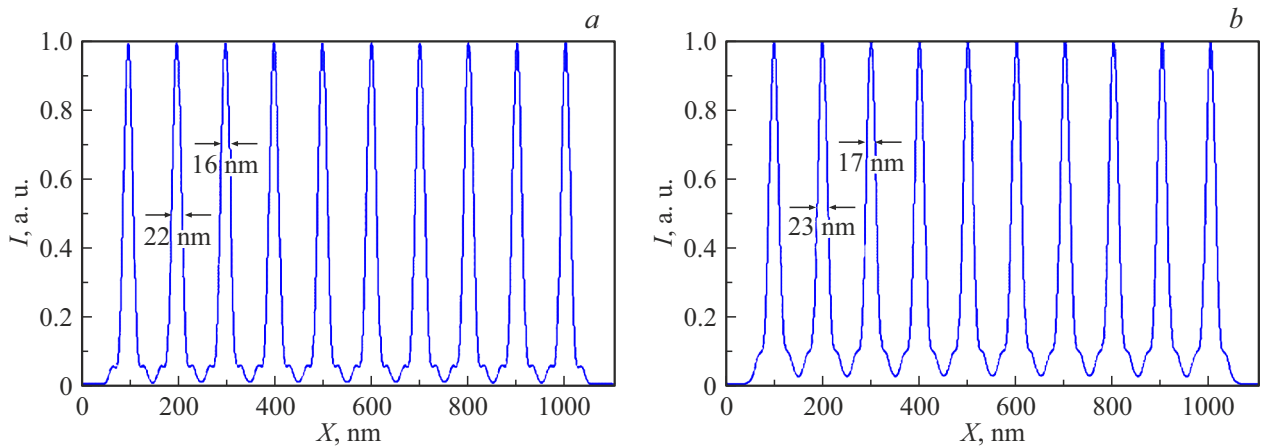


Figure 7. Cross sections of images of 200-nm holes of the dynamic mask. Lens $\times 10$, $\text{NA} = 0.3$, $\lambda = 11.2 \text{ nm}$. Incoherent radiation: *a* — in the center of the field of view, *b* — at the edge of the field of view $10 \times 10 \text{ mm}^2$.

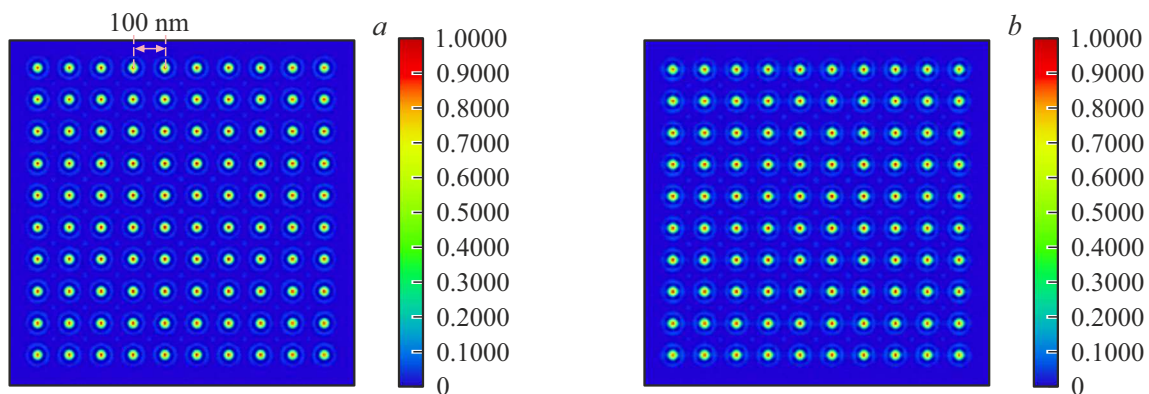


Figure 8. The image of 200-nm holes of a dynamic mask on a resist in the center (*a*) and at the edge (*b*) of the field of view $10 \times 10 \text{ mm}^2$. Lens $\times 10$, $\text{NA} = 0.3$, $\lambda = 11.2 \text{ nm}$. The synchrotron radiation was set to be coherent.

200-nm holes at the 0.7 level was 10 nm. The coherence of the radiation leads to low-intensity artifacts, which can be removed by selecting the sensitivity of the resist.

The optical circuit of the lens $\times 20$, $\text{NA} = 0.4$ is shown in Fig. 12. Circuit length — 1658 mm. The maximum

material removals for aspherization of mirrors amounted to 17.6 and $19.4 \mu\text{m}$ for M1 and M2, respectively. Such removals are possible with aspherization using ion beam etching systems [14]. The diameters of the mirrors were 174 and 66 mm.

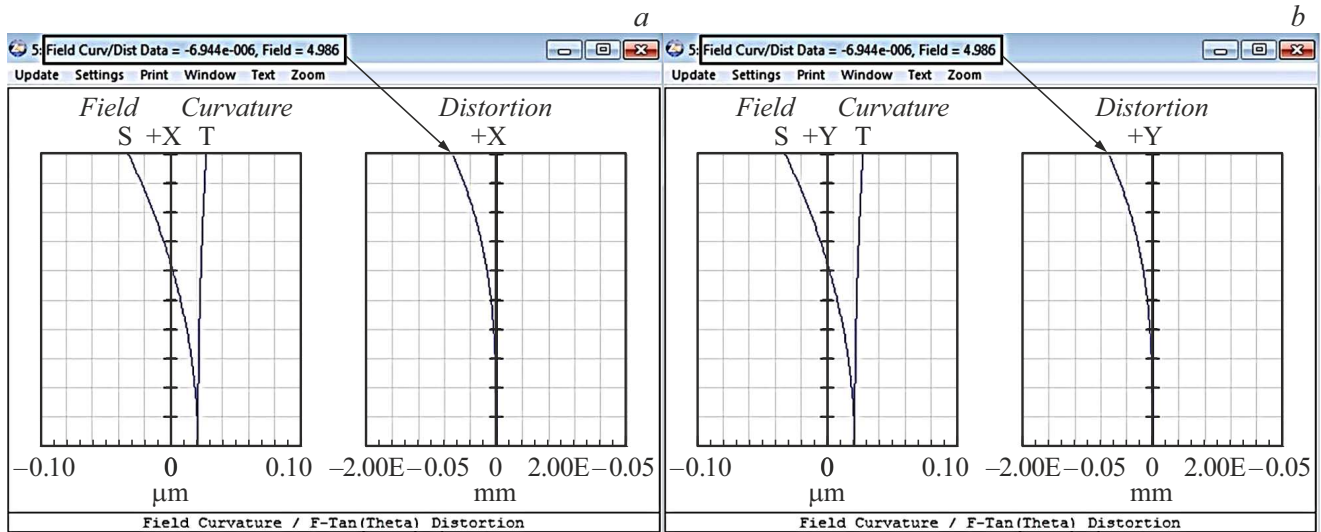


Figure 9. *a* — X-distortion, *b* — Y-distortion. Lens $\times 10$, NA= 0.3.

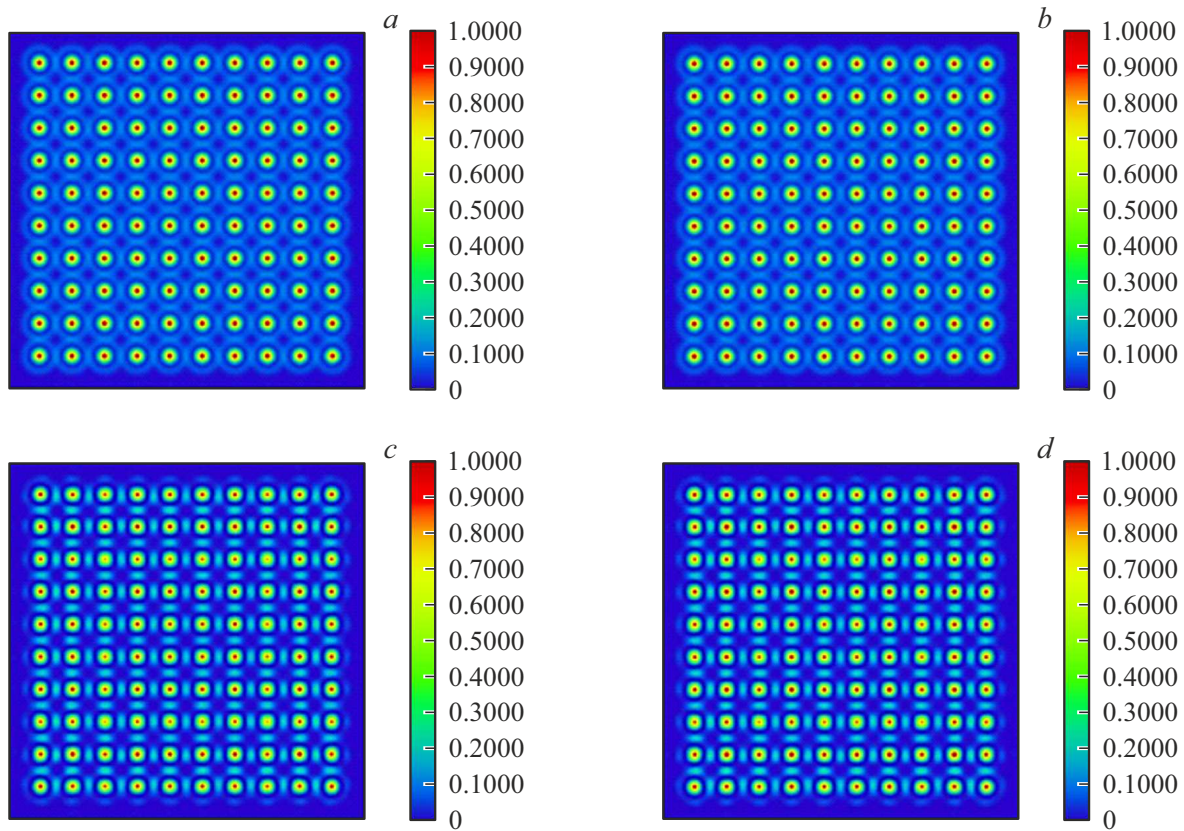


Figure 10. Image of a mask with 200-nm holes in the center and at the edge of the field of view. Lens $\times 20$, NA= 0.4, $\lambda = 11.2$ nm. Incoherent radiation: *a* — in the center of the lens field of view, *b* — at the edge of the field of view 10×10 mm². Coherent radiation: *c* — in the center of the lens field of view, *d* — at the edge of the field of view 10×10 mm².

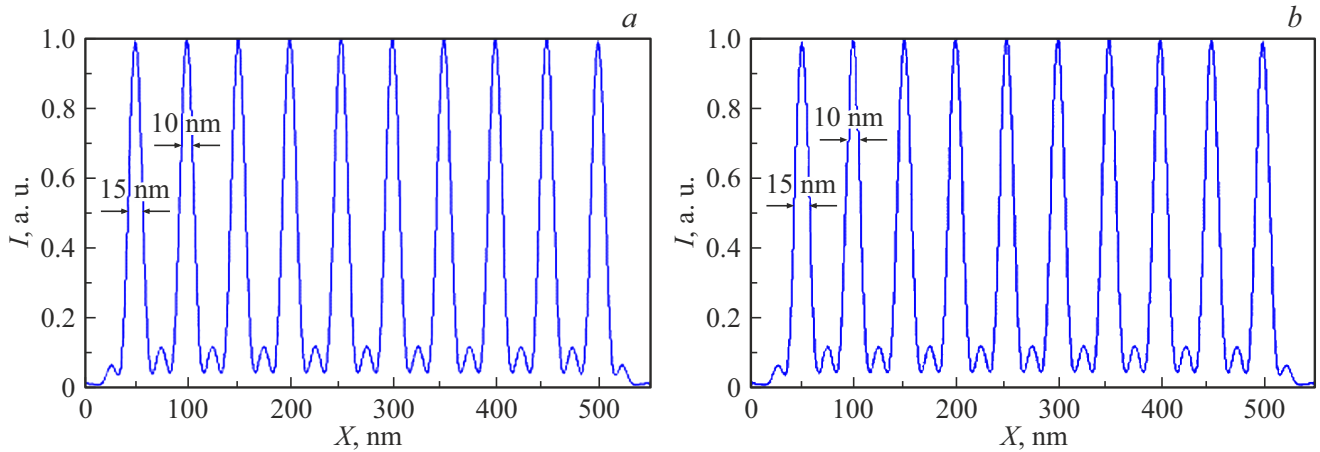


Figure 11. Cross sections of images of aperture openings. Lens $\times 20$, $NA=0.4$, $\lambda = 11.2$ nm. Incoherent light: *a* — in the center of the field of view, *b* — at the edge of the field of view 10×10 mm².

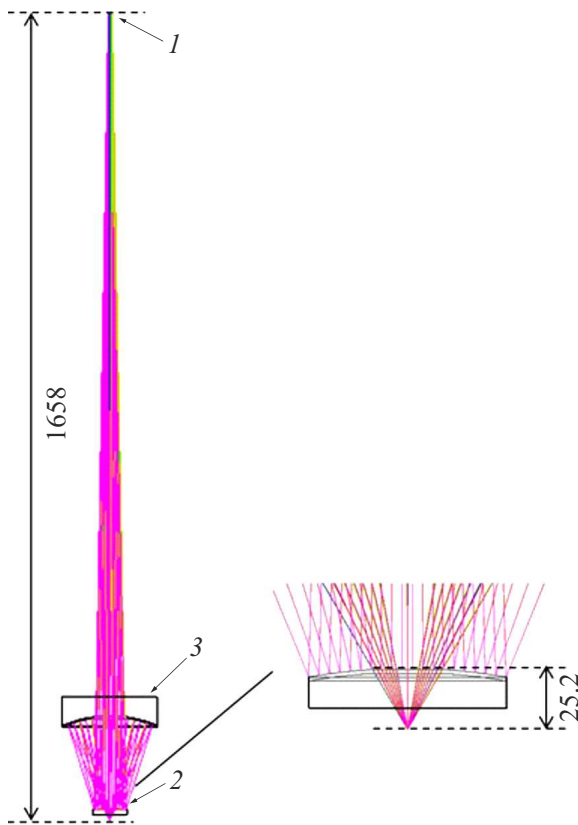


Figure 12. Lens $\times 20$, $NA=0.4$. *1* — dynamic mask, *2* — mirror M1 ($D_{optical} = 66$ mm, $R_{nearestsphere} = 244$ mm, $PV_{aspheric} = 17.6 \mu\text{m}$), *3* — mirror M2 ($D_{optical} = 174$ mm, $R_{nearestsphere} = 249.5$ mm, $PV_{aspheric} = 19.4 \mu\text{m}$).

Lens distortion $\times 20$, $NA=0.4$ is small — only 1.1 nm at the edge of the field of view, which is much smaller than the diameters of the hole images, so it almost does not affect the image (Fig. 13).

2. Evaluation of the productivity of lithographic circuit with a lens $\times 20$, $NA=0.4$

The radiation power at the output of the optical system can be represented as

$$P = E_{ph} \cdot \int_{E_1}^{E_2} S(E) \cdot R_1(E) \cdot R_2(E) \cdot R_3(E) \cdot R_4(E) \cdot T(E) dE, \quad (3)$$

where $S(E)$ — photon flux with energy in a single energy band E , E_{ph} — energy a photon with a wavelength of 11.2 nm and is equal to 108 eV, $R_i(E)$ — reflection coefficients of mirrors of the mask and lens illumination system taking into account the real roughness, $T(E)$ — filter transmittance to suppress long-wave radiation.

The functions $S(E)$ and $T(E)$ vary slightly on the Bragg width scale peaks, therefore, can be taken out for the sign of the integral. The number of photons exiting the system per second $N_{ph\ out}$ in the spectral bandpass of the optical system ΔE_{os} , expressed as a percentage of the central energy $E = 108$ eV can be represented as

$$N_{ph\ out} = s(108\text{eV})(\Delta E_{os}/0.1) \cdot R_1 \cdot R_2 \cdot R_3 \cdot R_4 \cdot T, \quad (4)$$

where R — peak reflection coefficients, T — filter transmission at photon energy 108 eV.

The number of photons that passed through the optical system is calculated by substituting into (4) the numerical value $s(108\text{eV}) = 6.2 \cdot 10^{12}$ [photon/(s·(0.1% bw))] (bw — bandwidth — bandwidth), taken from Fig. 14, $R_i = 0.7$, taken from [15,16], $T = 0.7$ — typical transmission value for beryllium-containing filters [17] and $\Delta E_{os} = 2.5\%$:

$$N_{ph\ out} = 6.2 \cdot 10^{12} \times 25 \times 0.7^4 \cdot 3.7 \cdot 10^{13} [\text{photon/s}], \quad (5)$$

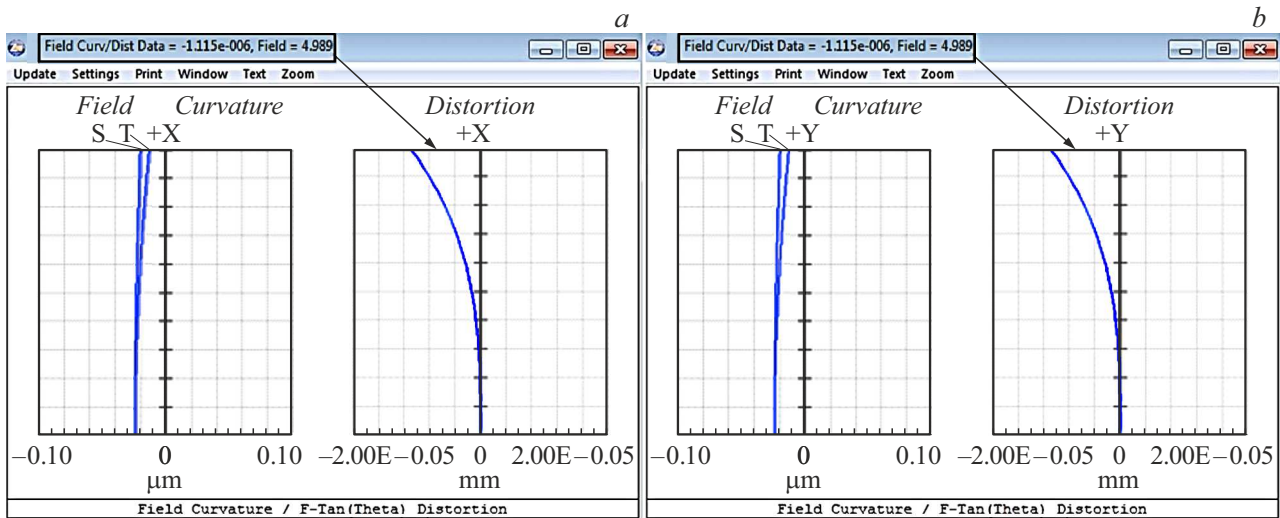


Figure 13. *a* — X-distortion, *b* — Y-distortion. Lens $\times 20$, NA= 0.4.

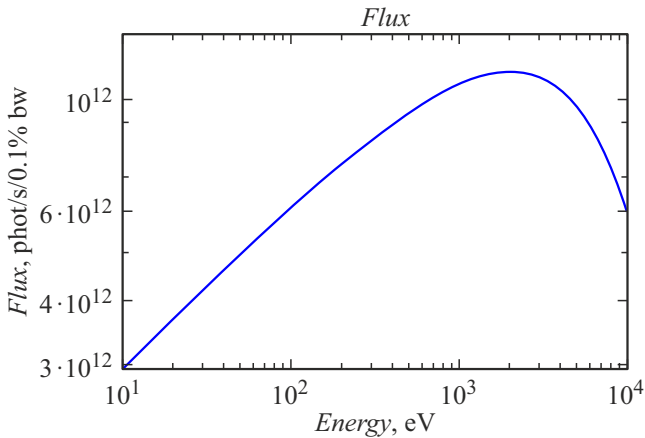


Figure 14. The photon flux in the „Large Storage Ring“ of the Kurchatov synchrotron, taken to evaluate the performance of the EUV lithograph (calculated in the OASIS [18] program).

X-ray intensity per PW plate:

$$P_W = 1.6 \cdot 10^{-19} \times 106 \times 3.7 \cdot 10^{13} = 6.4 \cdot 10^{-4} W, \quad (6)$$

The performance of the lithographic process $W[\text{cm}^2/\text{s}]$ with the sensitivity of the resist $S_{pr} = 10 \text{ mJ}/\text{cm}^2$ can be expressed as

$$W = P_W/S = 6.4 \cdot 10^{-2} \text{ cm}^2/\text{s} = 230[\text{cm}^2/\text{h}], \quad (7)$$

The following factors are not taken into account in formula (7):

- 1) according to Fig. 2, b, approximately 50% of the energy lies outside the dynamic mask region;
- 2) the diffraction losses of radiation at the hole are not taken into account, so expression (7) can be rewritten as

$$W = P_W/S \times DP = 230 \cdot DP[\text{cm}^2/\text{h}], \quad (8)$$

where DP is the fraction of radiation diffracted at the holes captured by the lens. For the circuits we considered: NA= 0.3, $\times 10$, $DP_1 = 0.48$; NA= 0.4, $\times 20$, $DP_2 = 0.25$;

3) the losses associated with the fact that not only the centers of the bands should receive the exposure dose, but also their edges can be estimated as $\sim 50\%$ based on Fig. 7.

The circuit NA = 0.3, $\times 10$ is the most productive and realistic from the point of view of further development at this stage of studies taking into account the above factors. Its performance will be $27.5 \text{ cm}^2/\text{h}$, approximately 0.35 plates with a diameter of 100 mm per h. This is quite sufficient performance for research tasks.

X-ray intensity losses during passage of a channel with a diameter of 200 nm and a length of 200–1000 nm in polysilicon are insignificant [19], therefore they may not be taken into account.

However, the greatest intensity losses can be expected due to the finite transparency of the dynamic mask — a fraction of the area occupied by the holes. Depending on the ratio of the width of the required lithographic tracks to the $\sim 20\text{-nm}$ diameter of the hole images, the performance decreases from 5 to 5^2 times, where 5 — is the ratio of $1 \mu\text{m}$ of the hole period to their 200-nm in diameter. The coefficient is 5 if 20-nm tracks are printed, 5^2 — if a continuous illumination of the resist is performed. Thus, the calculated productivity, taking into account all factors, ranges from 1/14 to 1/70 of a plate with a diameter of 100 mm per h.

Conclusions

1. The X-ray optical circuit of an X-ray maskless lithograph at a wavelength of 11.2 nm was calculated. Its main parameters were analyzed: the resolution and productivity of the lithographic process. It was shown that the circuit with NA= 0.3 and a reduction of $\times 10$ has the highest

productivity providing spatial resolution up to 17 nm with intensity level 0.7. It is necessary to use a lens with $NA=0.4$ and a reduction of $\times 20$ for achieving a 10-nm resolution.

2. It is possible to expose from 1/70 to 1/14 plates with a diameter of 100 mm per h using the synchrotron radiation of the Kurchatov Synchrotron which is sufficient for laboratory tasks.

3. It is necessary to use undulatory sources of synchrotron radiation to increase productivity, the brightness of which at the selected wavelength will be higher by 2–3 orders of magnitude. However, in this case, the thermal loads on the mask will increase many times, which will require additional studies and selection of materials.

Funding

The study was carried out with the financial support of the Russian Federation represented by the Ministry of Science and Higher Education, agreement № 075-15-2021-1350 dated October 5, 2021 (internal number 15.SYN.21.0004).

Conflict of interest

The authors declare that they have no conflict of interest.

References

- [1] H. Kinoshita, K. Kurihara, Y. Ishii, Y. Torii. *J. Vac. Sci. Technol. B: Microelectron. Processing and Phenomena*, **7** (6), 1648 (1989). DOI: 10.1116/1.584507
- [2] J.E. Bjorkholm, J. Bokor, L. Eichner, R.R. Freeman, J. Gregus, T.E. Jewell, W.M. Mansfield, A.A. Mac Dowell, E.L. Raab, W.T. Silfvast, L.H. Szeto, D.M. Tennant, W.K. Waskiewicz, D.L. White, D.L. Windt, O.R. Wood, J.H. Bruning. *J. Vac. Sci. Technol. B: Microelectron. Processing and Phenomena*, **8**, 1509 (1990). DOI: 10.1116/1.585106
- [3] G. Dattoli, A. Doria, G.P. Gallerano, L. Giannessi, K. Hesch, H.O. Moser, P.L. Ottaviani, E. Pellegrin, R. Rossmannith, R. Steininger, V. Saile, J. Wüst. *Nucl. Instr. Meth. Phys. Res. Section A: Accelerators, Spectrometers, Detectors and Associated Equipment*, **474** (3), 259 (2001).
- [4] A.N. Genselev, B.G. Goldenberg, V.F. Pindyurin. *Sposob provedeniya trafaretnoy skaniruyushchey sinkhrotronnoy rentgenovskoy litografii* (Institute of Nuclear Physics, SB RAS, Patent RU 2344454 C1, 2009.01.20) (in Russian).
- [5] K. Hesch, E. Pellegrin, R. Rossmannith, R. Steininger, V. Saile, J. Wüst, G. Dattoli, A. Doria, G.P. Gallerano, L. Giannessi, P.L. Ottaviani, H.O. Moser. *Conf.: Particle Accelerator Conference* (Chicago, PAC, **1**, 654, 2001), DOI: 10.1109/PAC.2001.987596
- [6] B. Jiang, Ch. Feng, Ch. Li, Z. Bai, W. Wan, D. Xiang, Q. Gu, K. Wang, Q. Zhang, D. Huang, S. Chen. *Scientific Reports*, **12**, 3325 (2022).
- [7] N. Choksi, D.S. Pickard, M. McCord, R.F.W. Pease, Y. Shroff, Y. Chen, W. Oldham, D. Markle. *J. Vac. Sci. Technol.*, **17**, 3047 (1999). DOI: 10.1116/1.590952
- [8] N.I. Chkhalo, V.N. Polkovnikov, N.N. Salashchenko, M.N. Toropov. *Proc. SPIE*, **10224**, 102241O-1-O8 (2016).
- [9] G.D. Demin, P.P. Kim, N.A. Dyuzhev. *Mater. XXVI Mezhdunarodnogo simpoziuma „Nanofizika i nanoelektronika“*, **1**, 544 (2022) (in Russian).
- [10] Electronic source. Available at: <http://kcsni.nrcki.ru/pages/main/sync/source/index.shtml>
- [11] A.D. Nikolenko, A.V. Bukhtiyarov, O.E. Tereshchenko, K.V. Zolotarev. *Mater. XXVI Mezhdunarodnogo simpoziuma „Nanofizika i nanoelektronika“*, **1**, 572 (2022) (in Russian).
- [12] I.V. Malyshev, A.E. Pestov, V.N. Polkovnikov, D.G. Renuov, M.N. Toropov, N.I. Chkhalo, Ya.V. Rakshun, Yu.V. Khomyakov, V.A. Chernov, I.A. Shchelokov. *Poverkhnost' Rentgenovskie, sinkhrotronnye i neytronnye issledovaniya* **5**, 3 (2023) (in Russian).
- [13] Electronic source. Available at: http://kcsni.nrcki.ru/files/pdf/otchet_2020.pdf
- [14] N.I. Chkhalo, I.A. Kaskov, I.V. Malyshev, M.S. Mikhaylenko, A.E. Pestov, V.N. Polkovnikov, N.N. Salashchenko, M.N. Toropov, I.G. Zabrodin. *Precision Engineer.*, **48**, 338 (2017). DOI: 10.1016/j.precisioneng.2017.01.004
- [15] M.V. Svechnikov, N.I. Chkhalo, S.A. Gusev, A.N. Nechay, D.E. Pariev, A.E. Pestov, V.N. Polkovnikov, D.A. Tatarskiy, N.N. Salashchenko, F. Schäfers, M.G. Sertsu, A. Sokolov, Y.A. Vainer, M.V. Zorina. *Opt. Expr.*, **26** (26), 33718 (2018). DOI: 10.1364/OE.26.033718
- [16] R.M. Smertin, N.I. Chkhalo, M.N. Drozdov, S.A. Garakhin, S.Yu. Zuev, V.N. Polkovnikov, N.N. Salashchenko, P.A. Yunin. *Opt. Expr.*, **30** (26), 46749 (2022).
- [17] N. Chkhalo, A. Lopatin, A. Nechay, D. Pariev, A. Pestov, V. Polkovnikov, N. Salashchenko, F. Schäfers, M. Sertsu, A. Sokolov, M. Svechnikov, N. Tsybin, S. Zuev. *J. Nanosci. Nanotechnol.*, **19**, 546 (2019). DOI: 10.1166/jnn.2019.16474
- [18] Electronic source. Available at: <https://www.aps.anl.gov/Science/Scientific-Software/OASYS>
- [19] P.Yu. Glagolev, N.A. Dyuzhev, V.I. Korneev, G.D. Demin. *Mater. XXVI Mezhdunarodnogo simpoziuma „Nanofizika i nanoelektronika“*, **2**, 843 (2023) (in Russian).

Translated by A.Akhtyamov